Journal of Structural Geology, Vol. 7, No. 6, pp. 737 to 749, 1985
Printed in Great Britain

0191-8141/85 $03.00 + 0.00

Effects of pressure on the micromechanics of faulting in San Marcos gabbro

TENG-FONG WONG and RONALD BIEGEL

Department of Earth and Space Sciences, State University of New York, Stony Brook, NY 11794, U.S.A.

(*Received* 17 *October* 1984; *accepted in revised form* 4 *March* 1985)

Abstract—Samples of San Marcos gabbro were deformed to both pre- and post-failure stages at confining pressures of 100, 250 and 350 MPa. Scanning electron microscope observations were performed on the samples after ion-milling. The unstressed gabbro has insignificant crack porosity but a high volume fraction of healed and sealed cracks. Extensive stress-induced cracking at high angles to the maximum compressive stress is observed at the two higher pressures. Such high-angle cracks are mostly associated with the pre-existing healed cracks or cleavage planes, and they control the geometry and length scale of crack networks in plagioclase. Intensive kinking in biotite is widely observed at 350 MPa pressure, which together with the crack networks control the brittle fracture process. Stress-induced cracks in samples deformed at 100 MPa pressure are predominantly subparallel to the maximum compressive stress, and their coalescence leads to shear localization.

Quantitative measurements of crack density as a function of differential stress indicate that crack interaction is appreciable beyond about 90% peak stress for all three pressures. The data also show significant decreases in stress-induced anisotropy as pressure increases, suggesting that there may be a threshold pressure beyond which stress-induced anisotropy vanishes with the onset of cataclasis.

INTRODUCTION

BRITTLE fracture of rock has been extensively investigated in the laboratory since the pioneer study by von Karman in 1911. The traditional approach has been to focus on measuring only one parameter, the fracture strength, which is the peak stress difference that a sample can sustain. An abundance of data has been accumulated on the fracture strength as a function of rock type, pressure, strain rate, pore fluid, loading rate, sample size and shape (Patterson 1978).

Empirical theories for brittle fracture (such as the Mohr and the Coulomb criteria) have provided much of the basis for the analysis of geological faulting as well as applied rock mechanics in engineering and mining. Although such theories have been interpreted in physical terms, they actually say very little about the physical mechanisms (Handin 1969). Because of the successful application of the Griffith theory in engineering fracture mechanics, early attempts to develop a physical theory of brittle fracture for rock (e.g. McClintock & Walsh 1962, Murrell & Digby 1970) are essentially mechanistic extensions of the classic work of Griffith (1920). Such modified Griffith theories assume that the development of macroscopic failure is due to the extension of a single microcrack with the critical dimension and orientation.

However, microstructural observations of experimentally deformed samples (Hallbauer *et al.* 1973, Sprunt & Brace 1974, Tapponnier & Brace 1976, Tullis & Yund 1977, Kranz 1980, Hadizadeh & Rutter 1982, Wong 1982a) show that the faulting process actually involves a multiplicity of microcracks and its essential nature lies not so much in the individual cracks as in the organization of the crack population and their interaction. The modified Griffith theories may be valid for the initiation process of individual microcracks, but they are not relevant to the process of microcrack coalescence to form a macroscopic shear fault.

In this context the scanning electron microscope (SEM) has been particularly effective in elucidating details of the micromechanics of brittle faulting. SEM studies on stress-induced cracking in the pre-failure stage (i.e. before the peak stress is reached and the onset of shear localization) by Tapponnier & Brace (1976) and Kranz (1979, 1980) clarified the relationship between microcrack growth and rock dilatancy. In many rocks the coalescence of microcracks culminating in a through-going fault occurs in the post-failure stage after the peak stress has been reached. Deformation in this stage is highly unstable, but Wong (1982a) was able to obtain a suite of post-failure samples for SEM study by using a test machine of high mechanical stiffness. His study on the Westerly granite shows that the faulting process involves several different instability mechanisms dependent on both mineralogy and grain orientation.

Such laboratory studies provide insight for the geological interpretation of faulting mechanisms at the outcrop scale (e.g Gay & Ortlepp 1979, Segall & Pollard 1983, Aydin & Johnson 1983). The experimental studies also provide useful criteria to distinguish between brittle and ductile deformation in naturally deformed samples (e.g. Anderson *et al.* 1983, Hadizadeh & Rutter, 1983, Mitra 1984).

Most of the previous studies have focused on granitic rocks or quartzites, and little is known about faulting mechanisms in basaltic and gabbroic rocks. Kronenberg & Shelton (1980) and Caristan (1982) recently considered Frederick diabase and outlined the role of microcracking in plagioclase and pyroxene in the brittle–ductile transition. We chose the San Marcos gabbro for the present study. Like the Westerly granite, the San Marcos gabbro is probably one of the crustal rocks most studied in experimental rock mechanics. Detailed measurements of fracture and frictional strength (Brace & Martin 1968, Stesky *et al.* 1974), dilatancy (Hadley 1973), electrical resistivity and fluid permeability (Brace & Orange 1968, Coyner *et al.* 1979), as well as a preliminary SEM study (Sprunt & Brace 1974) have been reported in the literature.

Our aim is to address a number of specific questions relevant to the micromechanics of faulting in the San Marcos gabbro. It is usually suggested that an increase in pressure can potentially stabilize microcracking, leading to a homogeneous distribution of stress-induced cracks, and ultimately to cataclastic flow (e.g. Ashby & Verrall 1977). However, Paterson (1978) in his recent review pointed out that 'it is not even clear that the physical processes on the microscopic scale are adequately understood . . . The greatest inadequacy of the theoretical situation is in treating the stabilization of the distributed microcracking that must occur initially in the cataclastic flow.' By performing SEM observation on complete suites of pre- and post-failure samples deformed over a wide range of pressure, we hope to gain insight into such micromechanical processes. We also characterized quantitatively the crack density and stress-induced anisotropy using stereological techniques previously developed (Wong in press), so that comparison can be made with recent theoretical analyses (e.g. Kachanov 1982, Moss & Gupta 1982, Nemat-Nasser & Horii 1984).

As we discuss below, the San Marcos gabbro has an unusually high concentration of healed and sealed cracks. Recent studies (e.g. Sprunt & Nur 1979, Padovani *et al.* 1982) have documented the extensive occurrence, both spatially and temporally, of such phenomena in many geological situations. These microstructures seem to be related to a range of geological problems from the interpretation of secondary fluid inclusions (Smith & Evans 1984) to in-situ stress measurements by overcoring (Engelder 1984). Deformation mechanisms have been proposed by which such healed/sealed cracks would preferentially fracture under tectonic stress and then be healed or sealed again in repeated cycles (Ramsay 1980, Cox & Etheridge 1983). A number of preliminary observations concerning the effects of stress on healed/sealed cracks are made in our study.

EXPERIMENTAL PROCEDURES

Deformation experiments

The samples were all cored from a single block of San Marcos gabbro. The sample geometry was cylindrical with diameter 15.8 mm and height 38.1 mm. The samples were pre-dried *in vacuo*, jacketed with polyurethane and deformed in a conventional triaxial configuration. The experiments were performed at W. F. Brace's laboratory at Massachusetts Institute of Technology.

All the samples were deformed at room temperature. The pressure medium was petroleum ether, and the confining pressure was monitored with a Heise gauge,

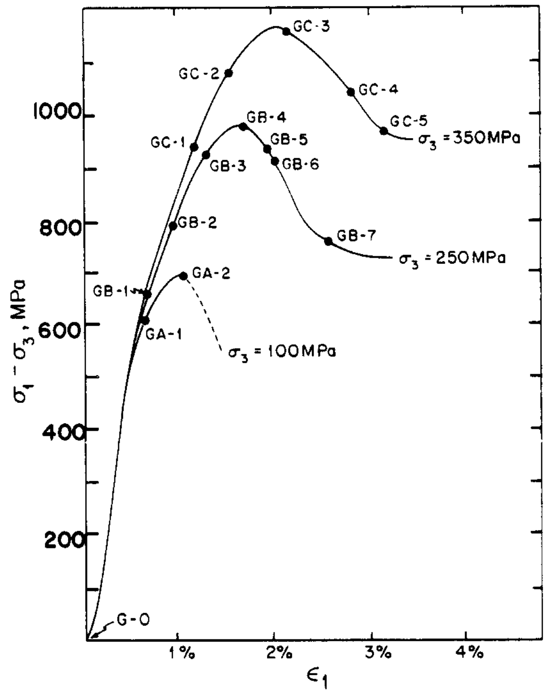

Fig. 1. Axial stress–strain curves showing the deformation history of all the specimens.

and maintained constant to within 1 MPa. The axial force was provided by a piston driven at a constant displacement rate by a ball-screw mechanism. The axial load was measured with an external load cell with a probable error of 2%. Previous studies (Brace & Martin 1968, Stesky *et al.* 1974) and our data show that the fracture strength of San Marcos gabbro as a function of pressure is highly reproducible. A constant strain rate of 10^{-5} s^{-1} was used. The displacement was measured outside the pressure vessel with a differential transformer (DCDT) mounted between the moving piston and the fixed lower platen. Measurements were accurate to within 1%. Elastic distortion of the loading system was 0.25 GN m^{-1}. This was subtracted from the apparent displacement recorded from the DCDT for calculation of the axial strain.

The post-failure behavior of San Marcos gabbro (Fig. 1) is relatively stable in comparison with those of other crystalline rocks previously investigated (e.g. Westerly granite and Frederick diabase). Using the same stiff machine discussed above, Wawersik & Brace (1971) and Wong (1982b) had to resort to manual unloading–loading control to stabilize the post-failure deformation of both Westerly granite and Frederick diabase. On the other hand, no post-failure instability was observed in this study for San Marcos gabbro at confining pressures of 250 MPa and above. Possible ambiguities in the interpretations of slip-weakening relations (Wong 1982b) and microstructural evolutions (Wong 1982a) in the post-failure stage in connection with cyclic unloading/loading are therefore avoided in this work.

The complete stress-strain curves shown here in Fig. 1 are those of GC-5 and GB-7. The failure is explosive at 100 MPa confining pressure; no attempt was made to use manual control to obtain the complete post-failure curve

Table 1. Stress history of samples

Sample*	σ_3(MPa)	σ_1–σ_3(GPa)
G-0	room	0
GA-1	100	0.63
GA-2	100	0.70
GB-1	250	0.67
GB-2	250	0.82
GB-3	250	0.94
GB-4	250	1.01
GB-5	250	0.96
GB-6	250	0.93
GB-7	250	0.77
GC-1	350	0.96
GC-2	350	1.11
GC-3	350	1.17
GC-4	350	1.06
GC-5	350	0.97

*All deformations were at room temperature.

and hence only a schematic, dashed curve is shown for the GA-series. The values of the confining pressure and differential stress to which the samples were subjected are tabulated in Table 1.

Electron microscopy

All deformed samples were set in epoxy, and sawed along a plane into two halves. Measurements using a micrometer show all the post-failure samples have azimuthal variation in dimension, indicating strain localization. Care was taken in such cases to saw along the plane with the most azimuthal dimensional increase.

Crack sections (25.4 mm in diameter and about 100 μm thick) were then prepared following the procedure outlined by Richter & Simmons (1977). The sections were then ion-milled (Brace *et al.* 1972) and sputter-coated with 0.02 μm of gold–palladium. Preliminary observations were made using an optical microscope, followed by detailed study with an I.S.I. Supra III scanning electron microscope. The latter is equipped with a secondary electron detector and a backscattered electron detector. Most micrographs shown here are secondary electron images unless otherwise specified in the figure captions. Compositional analysis could also be performed using a Princeton-Gamma Tech energy dispersive X-ray (EDX) analyzer.

Quantitative stereology

We used stereological techniques (Underwood 1970) to characterize quantitatively the stress-induced crack surface area for seven samples following procedures previously developed for axisymmetrically deformed rock samples (Wong 1982a, in press). Previous studies on Westerly granite used photo-mosaics at magnifications of about ×300. However, the abundance of healed cracks in the San Marcos gabbro renders it difficult to differentiate between open and closed cracks at such a magnification. Furthermore, the grain size of the gabbro is about three times that of the Westerly granite. It is therefore not feasible to prepare reasonably sized photo-mosaics with good resolution and yet at the same time capable of covering a representative area.

We decided to use a procedure similar to that of Kranz (1979) and obtain the data directly from the SEM. A line was marked on the CRT screen, and the number of crack intersections with the line were counted as the sample image moved across the screen along straight paths in different orientation. 18 traverses (of length 12 mm) would be taken along one particular orientation for every crack section. The spacing between adjacent traverses was 2/3 mm, and hence an area of 12 × 11.3 mm^2 (representing 30–40 grains) would be covered.

The number of intersections per unit length for each traverse was determined, and then statistical analysis was performed on the data for all traverses in a particular orientation. Both the mean and standard deviation were evaluated for such a population of 18 data. Crack counts were performed in two orthogonal directions for five deformed samples (GA-1, GB-1, GB-2, GC-1 and GC-2): the mean value of crack intersections per unit length for a direction parallel to maximum compression σ_1 is denoted as $P_L^{\parallel}$ whereas the mean value for a direction perpendicular to σ_1 (and hence parallel to σ_3) is denoted by $P_L^{\perp}$. An arbitrary set of two orthogonal directions were chosen for the virgin sample G-0. More detailed measurements of P_L as a function of orientation were made for one of the stressed samples (GB-3), for which P_L was determined at angles of 0, 30, 60 and 90° to σ_1.

The criterion for a crack count was that it should have an appreciable aperture at a magnification of ×1000. The SEM would be switched to higher magnifications if it was difficult to decide whether a crack was open or closed at a particular intersection. Almost equidimensional pores were not counted. Sealed and healed cracks were also excluded, except in the virgin sample where the sealed/healed cracks were counted separately and noted as such in the data.

OBSERVATIONS

Unstressed sample

A petrographical description of the San Marcos gabbro was given by Miller (1937). Our samples were cored from the same block used by Stesky *et al.* (1974) who provided the following modal analysis: 65% plagioclase, 12% biotite, 8% clinopyroxene, 7% amphibole (hornblende), 5% quartz and 3% oxides. The average grain size is 2 mm and porosity is 0.2%.

An abundance of healed and sealed cracks can be observed in sample G-0 under the SEM. We will follow the terminologies proposed by Richter & Simmons (1977). A crack is considered to be 'healed' if a previously open microcrack has been closed by precipitated material of composition similar to that of the host grain. Healed cracks are evidenced by bubble planes, fluid inclusions, and planes of solid inclusions. A crack is 'sealed' if it has been filled with secondary minerals mobilized from a distant origin.

Table 2. Crack density data*

Sample	$P_L^{\perp}$ (mm^{-1})	$P_L^{\parallel}$ (mm^{-1})	S_V (mm^2 mm^{-3})
G-0	0.26 ± 0.66†	0.27 ± 0.55†	0.54
G-0‡	5.91 ± 1.11†	6.93 ± 1.08†	12.84
GA-1	2.39 ± 0.81	1.15 ± 0.41	4.25
GB-1	0.51 ± 0.21	0.49 ± 0.19	0.99
GB-2	0.52 ± 0.27	0.45 ± 0.25	1.01
GB-3	2.64 ± 0.82	2.03 ± 0.56	5.02
GC-1	0.70 ± 0.37	0.61 ± 0.33	1.36
GC-2	2.72 ± 0.80	2.33 ± 0.54	5.27

*The symbols P_L and S_V are defined in equations (1)–(3).
†Measurements were for an arbitrary set of two orthogonal directions.
‡Data are for healed and sealed cracks.

To study the morphology and characterize quantitatively the density of the sealed and healed cracks is relatively simple in an undeformed sample due to the absence of stress-induced cracks. Most plagioclase grains have sets of healed cracks that appear as tabular inclusions, or bubble planes (Fig. 2). Our EDX analyses show that the inclusion material is probably slightly less sodic than the host plagioclase grain, but otherwise the compositions are very similar. Biotite grains also have healed cracks as tabular inclusions parallel to cleavage planes, and the EDX data also show that the two have similar compositions. The higher density of healed and sealed cracks seems to be in the pyroxene and hornblende grains (Fig. 3). The filling material usually shows a fibrous texture, but it is difficult to infer from the EDX data whether it is chlorite, serpentinite, or simply redeposited augite.

Very few open cracks can be observed under the SEM. Plagioclase has the least number of open cracks, some of which are quite long (up to 0.25 mm) with low aspect ratios. These are possibly along grain boundaries, but the high volume fraction of plagioclase in the gabbro renders it difficult unambiguously to locate grain boundaries under the SEM, even with the use of back-scattered mode. The almost equi-dimensional pores usually found in plagioclase in Westerly granite are seldom observed (Montgomery & Brace 1975). Relatively more open cracks can be observed in pyroxene and hornblende, usually associated with incomplete sealing or healing of pre-existing open cracks. Biotites seem to have the highest number of open cracks, most of which are along cleavage planes.

Stereological data were obtained along two arbitrary orientations perpendicular to each other. Measurements have been made separately for the open cracks as well as the healed/sealed cracks. The two sets of data are presented in Table 2.

Pre-failure samples

SEM observations were made on a total of six pre-failure samples (GA-1, GB-1, GB-2, GB-3, GC-2). Several modes of deformation are common to all the pre-failure samples even though they were deformed over a wide range of pressures from 100 and 350 MPa. The microcracks we observed are predominantly tensile so far as the SEM can resolve. Stress-induced cracks are found mostly in plagioclase and biotite. The microcracking in both phases occurs primarily by the opening of pre-existing healed cracks or by the propagation along favorably oriented cleavages. In this sense, the modes of deformation are similar to those previously documented for these two minerals in granitic rocks (e.g. Tapponier & Brace 1976, Kranz 1979). The healed and sealed cracks in pyroxene and hornblende can be observed to reopen also, but the crack densities are relatively low in comparison with those observed in plagioclase and biotite. Overall, the intensity of stress-induced cracking is less than that in samples of Westerly granite (Wong 1982a) deformed to similar degrees in the pre-failure region.

A key difference in the pre-failure stage between the GC-series and GA-series is in the lateral extent of en-échelon cracking. Whereas it is not uncommon to have arrays of several cracks propagating simultaneously along paths sub-parallel to one another without coalescence in GC-2 (e.g. Fig. 4) and to a lesser extent, in the GB-series, similar arrays of en-échelon cracks are rarely observed in GA-1. In the latter sample, a single crack can propagate over a grain of plagioclase or biotite in a direction sub-parallel to the maximum compression direction without appreciably activating additional cracking along a favorable cleavage plane or a healed crack nearby.

The stereological data reinforce the above qualitative observation. As shown in Fig. 5 and Table 2, the difference between $P_L^{\perp}$ and $P_L^{\parallel}$ is greatest for GA-1, showing that it has the most stress-induced anisotropy in microcrack distribution, and therefore most of the stress-induced cracks propagate along a direction parallel to σ_1.

Stress-induced cracking in pre-failure samples of the GB-series were quantitatively characterized in some

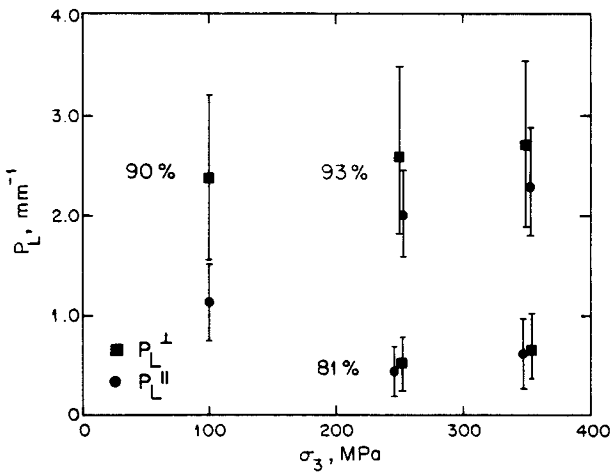

Fig. 5. The stereological parameter P_L as a function of pressure. The numbers next to the data indicate the differential stresses (as a percentage of peak value) to which the specimens were subjected.

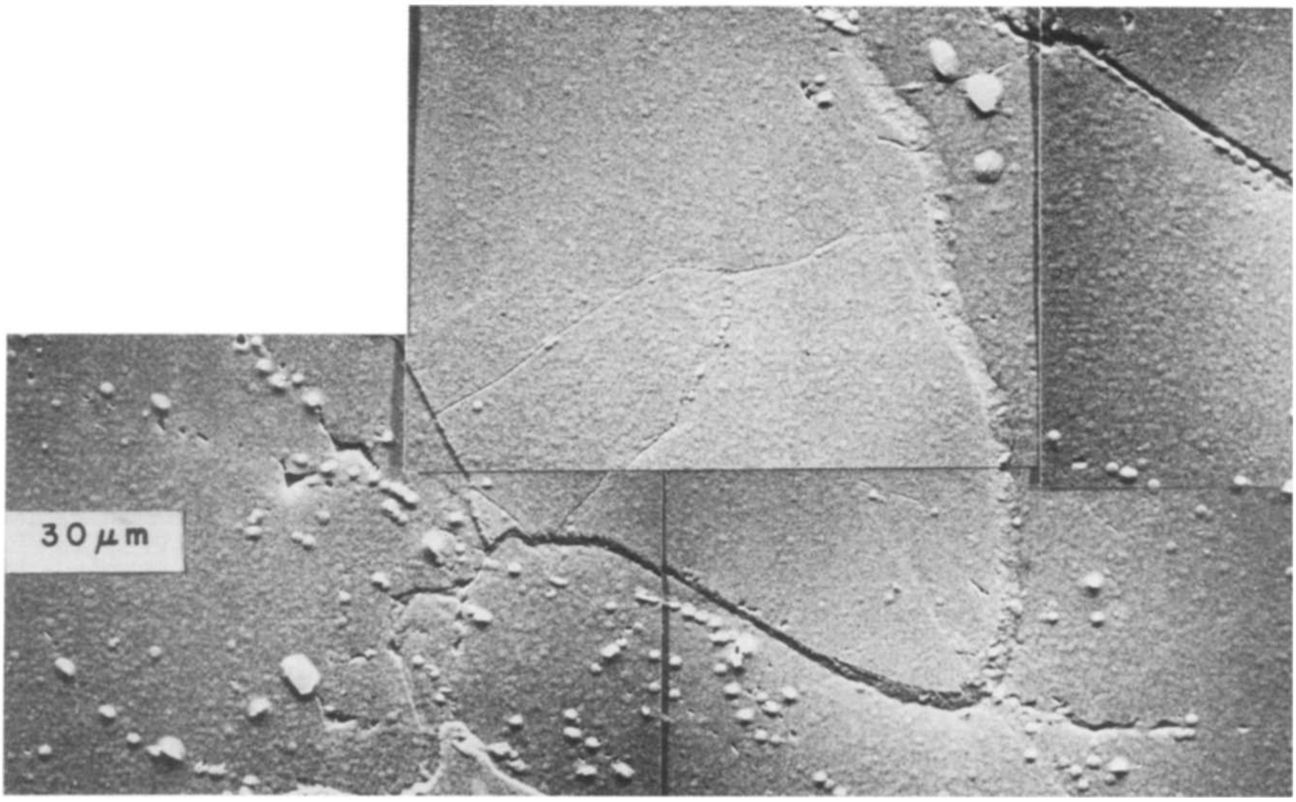

Fig. 2. Healed cracks observed in G-0. The host mineral is plagioclase. Note the arrays of 'bubbles' above the scale bar.

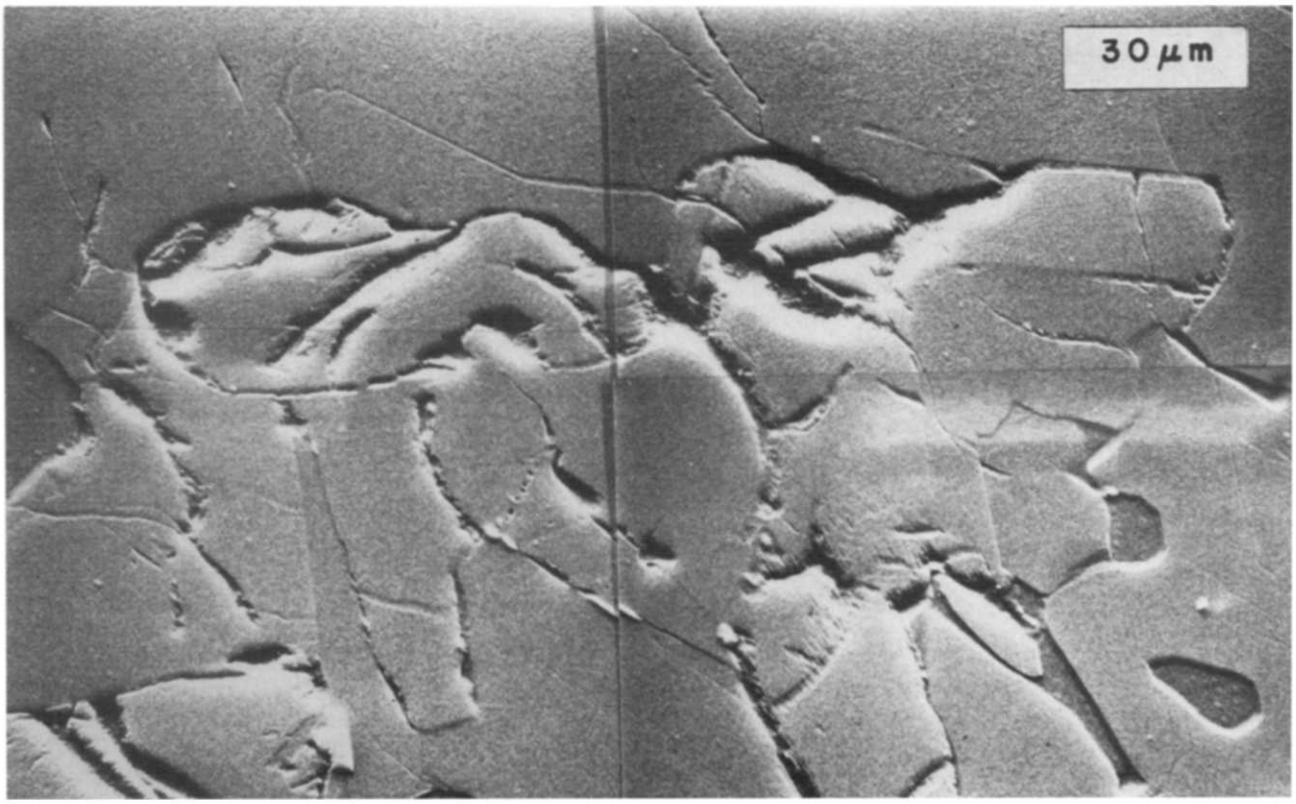

Fig. 3. Healed and sealed cracks in pyroxene observed in G-0. Note the fibrous textures of the inclusion material. The topography is due to differential rates of ion-thinning.

Fig. 4. Sub-parallel array of en-échelon cracks in plagioclase grain of GC-2. Note that a high proportion of the healed cracks have not re-opened. Maximum compression was vertical.

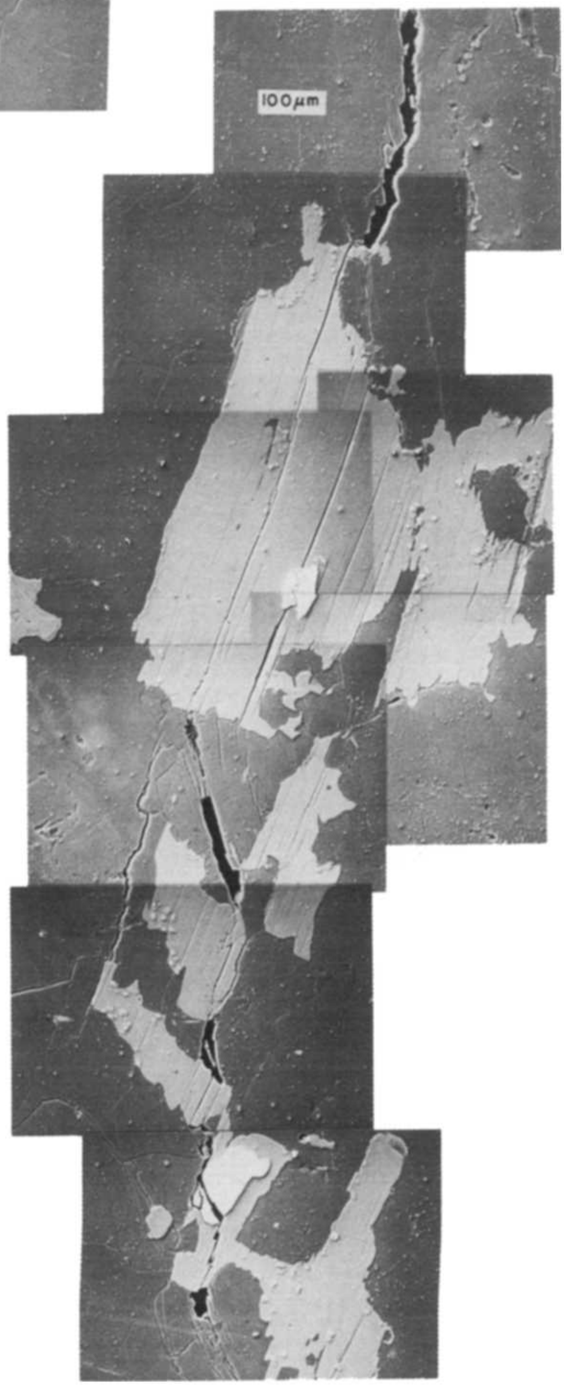

Fig. 8. Transgranular cracking sub-parallel to σ_1 extending over several biotite and plagioclase grains observed in GA-2. The lighter phase is biotite. Many of the healed cracks in both phases can be observed under high magnification to be still closed. Maximum compression was vertical (back-scattered electron image.)

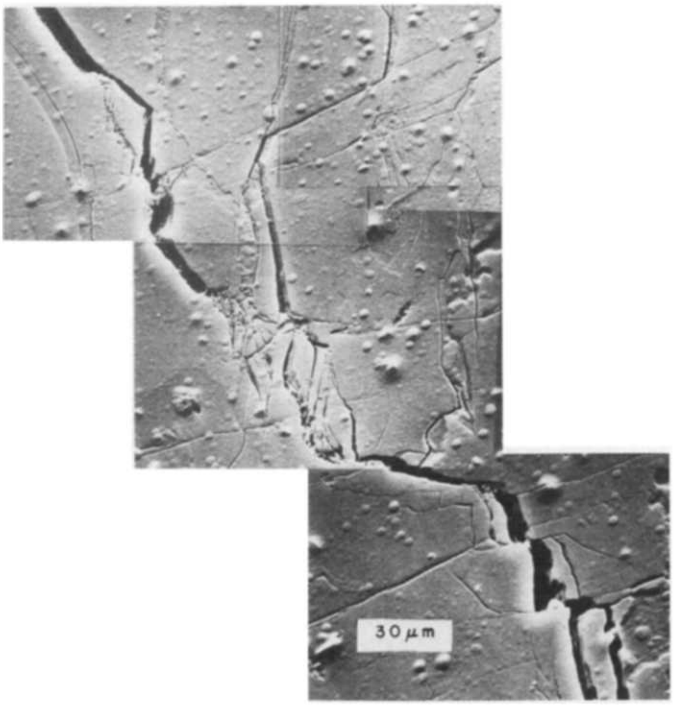

Fig. 9. Interruption of the propagation of a single crack across a plagioclase grain in GA-2. Note the irrational cleavages, rotation and crushing within the 'barrier' zone. Maximum compression was vertical.

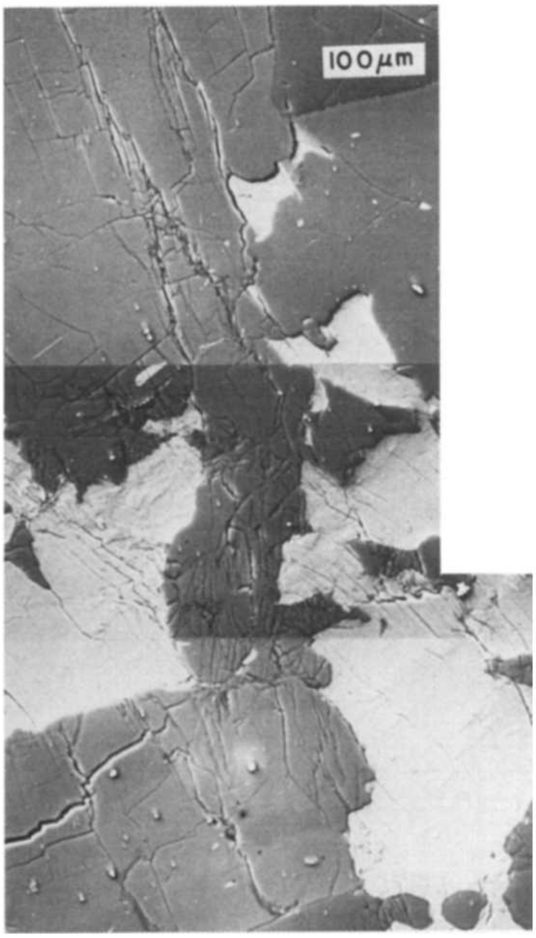

Fig. 10. Intensive kinking in biotite grains within a matrix of plagioclase in GC-3. Note the contrast in crack morphology between the zone in the immediate neighborhood of the two biotite grains and the zone above. Maximum compression was vertical (Back-scattered electron image).

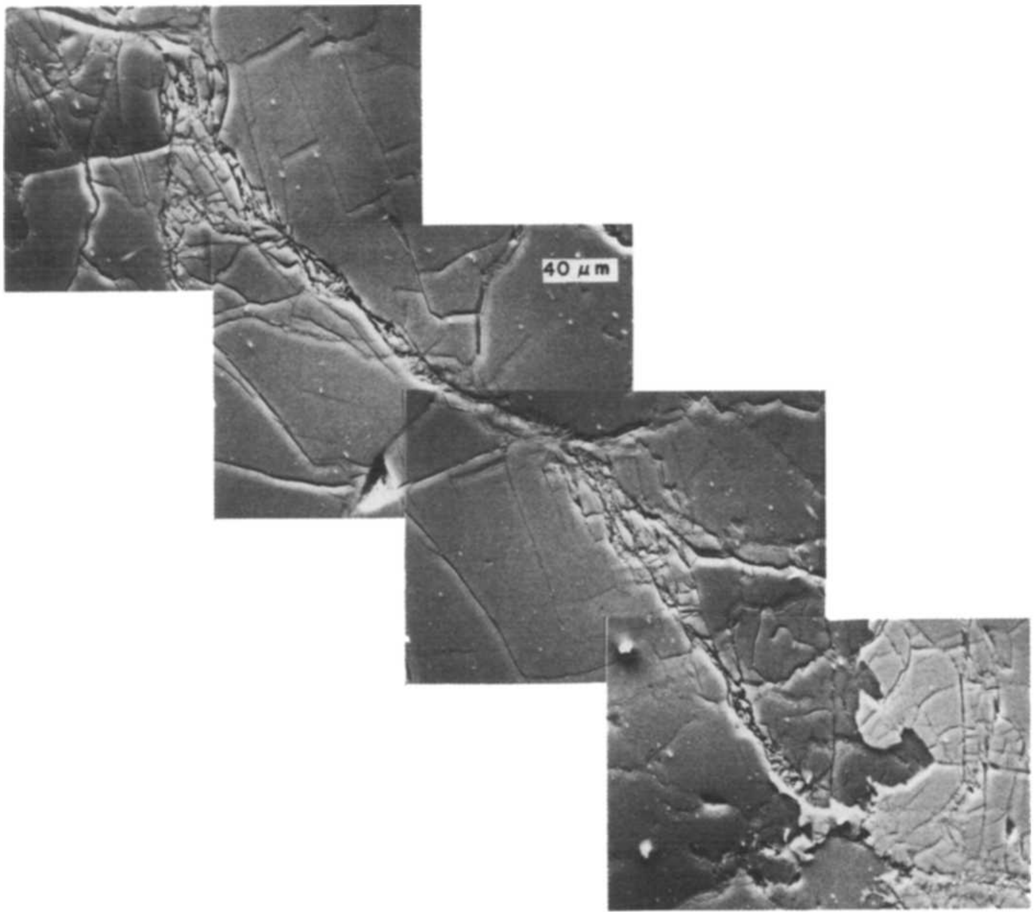

Fig. 11. An incipient localized zone extending all the way across a plagioclase grain in GC-3. Note the width of zone which persists over the whole length, and the intensive comminution within the zone. The relatively undeformed phase with a lighter color at the bottom is pyroxene. Maximum compression was vertical.

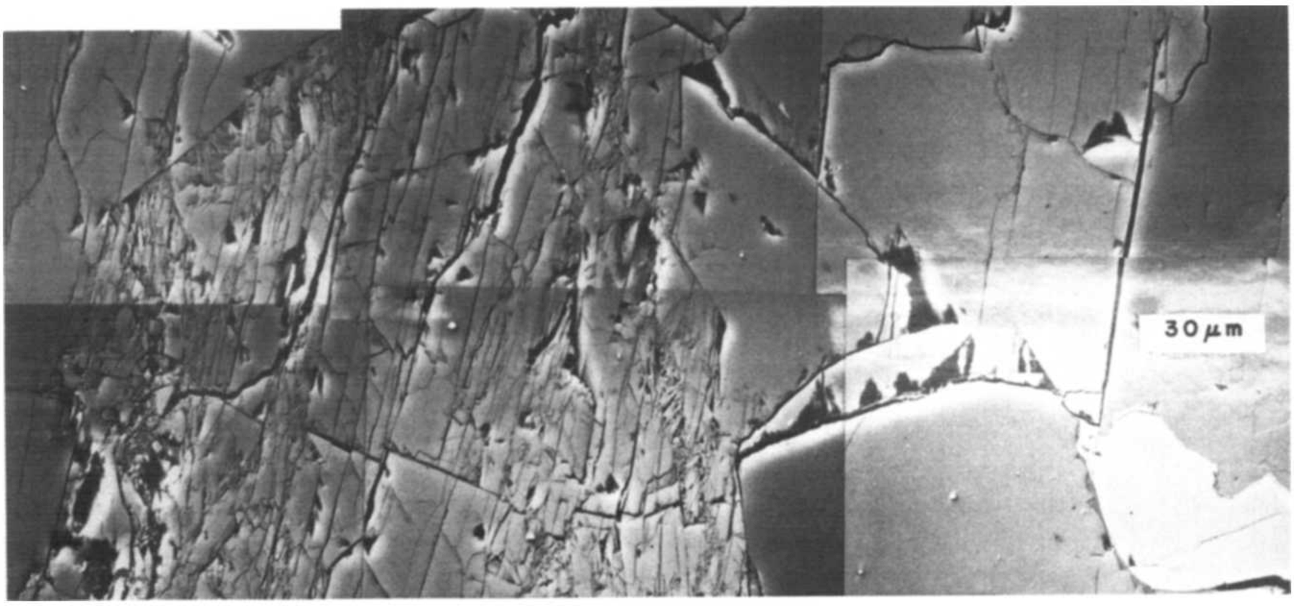

Fig. 12. Propagation of shear localization across a pyroxene grain in GB-5. Note the intensive comminution and grain size reduction. Maximum compression was vertical (back-scattered electron image).

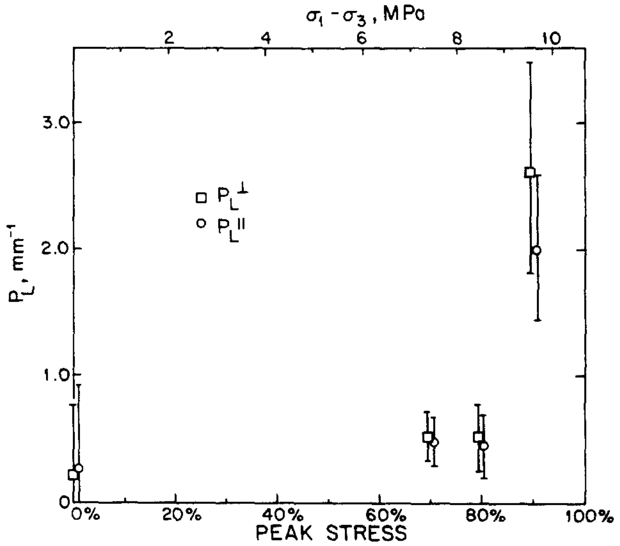

Fig. 6. P_L as a function of differential stress for the GB-series deformed under a confining pressure of 250 MPa.

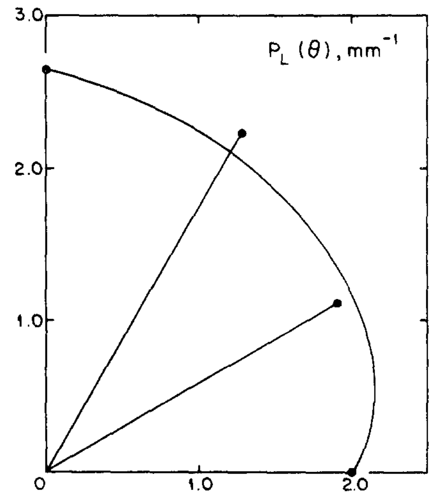

Fig. 7. A 'rose' diagram showing the angular dependence of $P_L(\theta)$. The solid line represents the theoretical curve for the sinusoidal relation [equation (1)].

detail. The data (Fig. 6) illustrate the evolution of crack density as a function of differential stress at 250 MPa confining pressure. A drastic increase of crack area (by as much as a factor of 5) can be observed between 80 and 93% of peak stress. The orientational dependence of P_L was also determined for GB-3 (Fig. 7) and the data indicate that a sinusoidal expression (Wong in press) is an appropriate approximation for $P_L(\theta)$.

Post-failure samples

Three samples (GA-2, GB-4 and GC-3) were retrieved just after the peak stress at each of the three confining pressures had been reached and a slight stress drop was detected in the stress record. The SEM observations on these three samples show that the grain boundaries have extensively opened. Most of the healed and sealed cracks in pyroxene and hornblende were also observed to open, but crack coalescence was not appreciable.

The mechanisms of microcrack interactions in both the plagioclase and the biotite in GA-2 are quite different from those in the other two samples. Sub-axial cracking seems to be the dominant mechanism in biotite and kinking is not significant. The most intense cracking in plagioclase was observed in the neighborhood of cleaved biotite grains, and transgranular cracks extending over two grains or more along a relatively straight path are quite common. The most dramatic situation extending over more than 2 mm is shown in Fig. 8. No throughgoing fault has formed, and most of the incipient localized zones tend to stop at local barriers within grains (Fig. 9). Such local zones are usually cleaved along irrational directions into small blocks, and deformation has to be accommodated by rotation and crushing of the blocks.

A high percentage of the biotite grains in GC-3 have experienced intensive kinking. To accommodate the high plastic strain associated with the kink bands, neighbouring plagioclase grains have deformed by microfracturing in various directions, along cleavage planes and by opening most of the pre-existing healed cracks (Fig. 10). Significant interaction and coalescence can be observed among en-échelon cracks in plagioclase which previously constituted a sub-parallel array in the pre-failure stage (Figs. 10 and 11). As a consequence, several incipient localized zones (with a lateral extent of 20 m or so) have propagated over 1–2 grains. The material within such zones is again segmented by microcrack networks into small blocks and shear deformation is accompanied by rotation, crushing and comminution.

Deformation mechanisms in GB-4 are qualitatively similar to those in GC-3. Three of the post-failure samples (GC-4, GC-5 and GB-7) have throughgoing faults, and therefore the useful SEM observations on the latter stages of post-failure deformation were solely obtained from GB-5 and GB-6.

Crack coalescence leading to shear localization can finally be observed in both the pyroxene and the hornblende (Fig. 12) in GB-5 and GB-6. Nearly all the biotite grains experienced intensive kinking and gouge formation has commenced within plagioclase grains.

DISCUSSION

Interpretation of the stereological data

Various approaches have been taken to characterize quantitatively microcrack density in deformed samples, and a comprehensive review was recently presented by Kranz (1983). We decided to employ standard techniques from quantitative stereology (Underwood 1970) in our previous work (Wong 1982a, 1982c) primarily because of the convenience of the techniques and the simplicity with which the data can be interpreted physically. The stereological parameter P_L is related to the crack surface per unit volume (S_V), a natural parameter to use in analyzing the energetics of deformation involving microcracking (Wong 1982c). Recent theoretical models developed by Walsh (Walsh & Grosenbaugh 1979, Walsh 1981, Walsh & Brace 1984) show that S_V, together with the statistical distribution of crack apertures, determine the pressure dependence of a range of mechanical and transport properties including compressibility, permeability and electrical conductivity.

Our previous measurements for stressed samples of Westerly granite at relatively low magnifications ($\times 150$ or $\times 300$) suggest that $P_L(\theta)$ for an axisymmetrically compressed sample in the pre-failure stage can be approximated quite well by the following sinusoidal relation

$$P_L(\theta) = P_L^{\parallel} + (P_L^{\perp} - P_L^{\parallel}) \sin \theta, \qquad (1)$$

where $P_L(\theta)$ is the number of crack intersections per unit length of a reference grid oriented at angle θ to σ_1. $P_L^{\parallel}$ and $P_L^{\perp}$ denote $P_L(0)$ and $P_L(\pi/2)$, respectively. Our data for GB-3 at a higher magnification of $\times 1000$ show that a similar approximation would also be appropriate for San Marcos gabbro (Fig. 7).

More complicated functions can be used (Philofsky & Hilliard 1969) but they would probably not improve the resolution due to the spatial heterogeneity in microcrack distribution as indicated by the standard deviation in our data (Table 2). The physical motivation for the above sinusoidal expression is that one can show by geometric probability arguments that the orientational dependence of crack surface per unit volume $S_V(\theta, \omega)$ is given by

$$S_V(\theta, \omega) = \frac{P_L^{\parallel}}{\pi} + \frac{P_L^{\perp} - P_L^{\parallel}}{2} \delta\left(\theta - \frac{\pi}{2}\right). \qquad (2)$$

Here $\delta(\theta)$ is the Dirac delta, ω is the azimuthal angle and axisymmetry is reflected by the fact that the right hand side has no dependence on ω. The physical interpretation is thus simply that the pore space can be divided into two sets of microcracks, one of which is composed of randomly oriented surfaces embedded in a rock matrix, and the other a set of microcracks aligned with their normals at right angles to σ_1 (i.e. with the crack surface parallel to σ_1). The total crack surface per unit volume is then given by

$$S_V = \int_0^{\pi} d\omega \int_0^{\pi} S_V(\theta, \omega) \sin \theta \, d\theta$$

$$= \frac{\pi}{2} P_L^{\perp} + \left(2 - \frac{\pi}{2}\right) P_L^{\parallel}. \qquad (3)$$

Note that the opposite sides of a crack surface are counted as one here, and S_V multiplied by the fracture mechanics parameter, G_{Ic} (the critical energy release rate under mode I) determine the fracture energy per unit volume for tensile cracking. Table 2 includes all the calculated values of S_V using equation (3) for our samples.

Effects of pressure on the micromechanics of faulting

The deformation of San Marcos gabbro here we consider is unquestionably in the brittle field. The peak stress has a strong dependence on pressure, samples deformed well into the post-failure stage all show a throughgoing fault at about 32° to σ_1, and some of our unpublished data on inelastic volume change show appreciable dilatancy (of several per cent) prior to failure at all three confining pressures. Our SEM observations and stereological data suggest that even within the brittle field, the confining pressure has significant effects on both the orientational and spatial distribution of stress-induced microcracking.

Previous work has concluded that stress-induced crack density accumulated prior to failure increases with confining pressure in granites (Wawersik & Brace 1971, Kranz 1980, Wong 1982a) and carbonate rocks (Hugman & Friedman 1979). The San Marcos gabbro data presented here reflect the same trend (Table 2 and Fig. 5).

It was suggested that stress-induced anisotropy would decrease with confining pressure, but the previous data were either for a relatively narrow range of pressure (Wawersik & Brace 1971) or for deformation under the coupled effects of pressure and temperature (Wong 1982a). The present set of data (Fig. 6) show clearly a reduction of the difference between $P_L^{\perp}$ and $P_L^{\parallel}$ (at about 90% of peak stress) with increasing confining pressure. Since this difference is proportional to the total area of those stress-induced cracks with a preferred orientation parallel to σ_1 [see equation (2) above], one may extrapolate and conclude that there is a critical pressure above which $P_L^{\perp}$ equals $P_L^{\parallel}$ implying isotropically distributed microcracking (i.e. cataclastic flow).

Our SEM observations provide details on the effects of pressure on the micromechanical processes, particularly those in biotite and plagioclase. Tapponnier & Brace (1976) have conjectured that plastic flow and ultimately kinking in biotite might be the key instability process to trigger shear localization. Their model was based on SEM observation of deformation in Westerly granite, primarily in the pre-failure stage. However, the detailed observations on post-failure samples of the same rock by Wong (1982a) show that several instability mechanisms are operative in the feldspars as well as the biotite to bring about the onset of localization. The dominant role of the biotite which we observed in the initiation of localization in San Marcos gabbro (Figs. 8 and 10) is quite similar to that originally proposed by Tapponier & Brace for the Westerly granite. This is not surprising because the former has about 12% biotite whereas the latter has only 5%.

Our observations indicate that many non-coalescing, sub-parallel arrays of en-échelon cracks can be found in plagioclase in pre-failure samples of the GB and GC series. Furthermore, the incipient localized zones made up of comminuted plagioclase blocks in the post-failure samples were observed to widen with pressure. (Compare Figs. 9 and 11.) The former observation is in agreement with the theoretical prediction of a number of fracture mechanics models (e.g. Kachanov 1982, Nemat-Nasser & Horii 1982) that pressure would stabilize the extension of cracks along the maximum compression direction. However, the situation here may be more complicated than assumed in such models. Our observations clearly indicate that pre-existing planes of weakness (along cleavages or healed/sealed cracks) exert considerable influence on the paths of crack propagation in the gabbro. Therefore, the usual assumption on isotropy of fracture toughness may not be appropriate.

The widening of the incipient localized zones in plagioclase is probably also related to the large plastic strain associated with the biotite kink bands observed in the high pressure samples. Microfracturing in plagioclase has been extensively documented to occur in both laboratory (e.g Tullis & Yund 1977, Kronenberg & Shelton 1980, Caristan 1982) and naturally (e.g. Mitra 1978, Boullier 1980, Hanmer 1982) deformed samples over an anomalously wide range of pressure and temperature conditions. This is attributed to the fact that plagioclase usually has a plastic yield stress which is higher than that of the other phases in an aggregate. The interaction of plastic flow in biotite with microcracking and comminution in plagioclase which has been documented here is probably quite similar to the micromechanisms in other situations, such as the microfracturing in plagioclase induced by plastic flow in neighbouring quartz grains in a quartzo-feldspathic rock.

A quantitative comparison between our stereological data and the theoretical predictions of micromechanical models was performed and the details are presented elsewhere (Wong in press). The analyses show that the stress-induced anisotropy in microcrack distribution as predicted by the 'sliding crack' model (e.g. Nemat-Nasser & Horii 1982, Steif 1984) agrees quite well with the stereological data. Furthermore, energetic considerations indicate that the inelastic energy of the gabbro samples deformed at pressures above 250 MPa cannot be dissipated solely by tensile microcracking. Plastic energy taken up by kinking instability (involving a plastic strain of several per cent) or frictional dissipation (involving shear slip of several μm) can explain both the quantitative SEM observations and the macroscopic stress–strain data.

Although our stereological data suggest an asymptotic approach to cataclastic flow as the confining pressure increases further, it is not possible to extrapolate and speculate on the value of the threshold pressure for the onset of homogeneous cataclasis. Unlike calcite rocks, which can usually deform by cataclastic flow under moderately high pressures at room temperature (see review by Paterson 1978), some silicate rocks of low porosity have been known to stay in the brittle field under pressures up to 3 GPa in the absence of elevated temperature. Schock & Heard (1974) reported that Westerly granite failed in a brittle manner at pressures up to 2 GPa, and Shimada *et al.* (1983) also observed brittle fracture in Man-nari granite, Murotomisaki gabbro, Horoman dunite, and Akaishi eclogite at pressures up to 3 GPa at room temperature. On the other hand, Byerlee (1968) reported the occurrence of the brittle–ductile transition for two serpentine-bearing rocks (Spruce Pine dunite and Nahant gabbro) at a confining pressure of only 500 MPa, and Hadizadeh & Rutter (1983) recently observed the transition to cataclastic flow for an orthosilicate (with a relatively high porosity of 7.4%) at 600 MPa pressure.

Opening of healed and sealed cracks under the action of stress

There have been a number of recent studies on the morphology and geochemistry of healed and sealed cracks. However, there is to our knowledge no quantitative study of the density of such microstructures. Our stereological data (Table 2) on the healed/sealed cracks observed in the unstressed sample along two orthogonal directions show a small amount of anisotropy. The value of crack surface area per unit rock volume for the healed/sealed cracks is amazingly high: it is two to three times the surface area of cracks we observed in all the samples deformed to about 93% peak stress. The relatively isotropic distribution of healed and sealed cracks suggests that the initial opening of such cracks was thermal in origin, probably induced by internal stresses due to thermal expansion mismatch or thermal expansion anisotropy (Nur & Simmons 1970). Microcracking due to tectonic stresses would be expected to result in more appreciable anisotropy. The relatively high value for the volume fraction we observed is not unusual in thermally cracked samples of crustal rocks (Fredrich & Wong 1984).

The healing and sealing of microcracks seem to be quite common in gabbroic rocks. Wang & Simmons (1978) concluded that the gabbroic core from 5.3 km depth beneath the center of the Michigan Basin they analyzed contained few open cracks. Anomalously low permeability values (down to nanodarcies) have been reported for San Marcos gabbro (Coyner *et al.* 1979) and Creighton gabbro (Trimmer *et al.* 1980), probably a consequence of the abundance of healed and sealed cracks.

Kranz (1983), in his recent review, listed several mechanisms documented in the literature by which local strength can be reduced resulting in microcrack propagation along certain preferred surfaces which include cleavage planes, grain boundaries, as well as any surfaces accessible to fluid and vulnerable to stress corrosion. Our observations here indicate that pre-existing healed and sealed cracks are also preferred surfaces for stress-induced crack propagation, and that healed and sealed cracks can influence the microcrack growth to an extent at least comparable to cleavage planes.

Hadley (1973), in discussing the complications related to the determination of the value of stress at the onset of dilatancy, pointed out that the stress-volumetric strain curves for San Marcos gabbro generally exhibited two regions of linear behavior with distinct slopes. It is possible that this unusual bilinear behavior is somehow related to the deformation of the healed/sealed cracks, and further work has to be done to clarify this.

Our recent SEM observations on preheated samples of Frederick diabase show that the healed and sealed crack surfaces are also favorable locations for the initial development of thermally induced cracking (Fredrich & Wong 1984). Some aspects of microcrack morphology in experimentally deformed samples of Frederick diabase reported by Kronenberg & Shelton (1980) and Caristan (1982) should probably be interpreted taking into consideration the roles of the healed and sealed cracks.

CONCLUSION

We focus on the effects of pressure on the micromechanics of brittle faulting in San Marcos gabbro in the present study. The use of quantitative stereology here to characterize the stress-induced cracking is more extensive and thorough than most previous work. Our study reinforces the suggestion (Wong in press) that such an approach provides an efficient technique to quantify the physics of brittle fracture. We conclude from the stereological data that the stress-induced crack surface area increases whereas the stress-induced anisotropy decreases as a function of pressure.

The previous study by Wong (1982a) has concluded that not one, but several instability mechanisms, dependent on both mineralogy and grain orientation, are usually operative leading to shear localization. Similar trends are observed in San Marcos gabbro, but the overall behavior is not as complex as that in Westerly granite. Quartz (which does not have a preferred cleavage plane) is absent, and all the major phases of the gabbro have cleavages. The equant pores, an abundance of which are usually found in plagioclase in Westerly granite with significant influence on crack propagation and coalescence, are infrequently observed here.

Our qualitative observations show that the deformation mechanism in biotite goes through a transition from predominantly brittle cracking to kink band formation with increasing pressure, and the onset of instability in this phase plays a significant role in the initiation of shear localization. Cleavages in plagioclase, clinopyroxene and hornblende are preferred planes for stress-induced cracking as previously suggested. In addition, we conclude that pre-existing healed and sealed cracks exert significant control over the geometry of crack growth, and that at least for the case of San Marcos gabbro, their influence on the micromechanical processes is comparable to that of the easy cleavages.

Acknowledgements—One of us (T-f. W.) would like to thank Bill Brace for providing laboratory facilities for the deformation experiments and also Brian Evans for helpful discussions on crack-healing mechanisms. Two anonymous reviewers provided helpful suggestions on the manuscript. This research was supported by the National Science Foundation under grant EAR82-18379 and by the University Award Program of the State University of New York.

REFERENCES

Anderson, J. L., Osborne, R. H. & Palmer, D. F. 1983. Cataclastic rocks of the San Gabriel fault—an expression of deformation at deeper crustal levels in the San Andreas fault zone. *Tectonophysics* **98**, 209–251.

Ashby, M. F. & Verrall, R. A. 1977. Micramechanisms of flow and fracture, and their relevance to the rheology of the upper mantle. *Phil. Trans. R. Soc.* **A288**, 59–95.

Aydin, A. & Johnson, A. M. 1983. Analysis of faulting in porous sandstones. *J. Struct. Geol.* **5**, 19–31.

Boullier, A. M. 1980. A preliminary study on the behavior of brittle minerals in a ductile matrix: examples of zircons and feldspars. *J. Struct. Geol.* **2**, 211–217.

Brace, W. F. & Martin, R. J., III. 1968. A test of the law of effective stress for crystalline rocks of low porosity. *Int. J. Rock Mech. Min. Sci.* **5**, 415–426.

Brace, W. F. & Orange, A. S. 1968. Further studies on the effects of pressure on electrical resistivity of rocks. *J. geophys. Res.* **73**, 4507–5420.

Brace, W. F., Silver, E., Hadley, K. & Goetze, C. 1972. Cracks and pores—a closer look. *Science, Wash.* **178**, 163–165.

Byerlee, J. D. 1968. Brittle–ductile transition in rocks. *J. geophys. Res.* **73**, 4741–4750.

Caristan, Y. 1982. The transition from high temperature creep to fracture in Maryland diabase. *J. geophys. Res.* **87**, 6781–6790.

Cox, S. F. & Etheridge, M. A. 1983. Crack-seal fibre growth mechanisms and their significance in the development of oriented layer silicate microstructures. *Tectonophysics* **92**, 147–170.

Coyner, K. B., Brace, W. F. & Walsh, J. B. 1979. New laboratory measurements of permeability and electrical resistivity of crystalline rocks (abstract). *Trans. Am. geophys. Un* **60**, 943.

Engelder, T. 1984. The time-dependent strain relaxation of Algerie granite. *Int. J. Rock Mech. Min. Sci.* **21**, 63–73.

Fredrich, J. & Wong, T-f. 1984. Dependence of surface area of thermal cracks on temperature (abstract). *Trans. Am. geophys Un* **65**, 1074.

Gay, N. C. & Ortlepp, W. D. 1979. Anatomy of a mining induced fault zone. *Bull. geol. Soc. Am.* **90**, 47–58.

Griffith, A. A. 1920. The phenomena of rupture and flow in solids. *Phil. Trans. R. Soc.* **A221**, 163–198.

Hadizadeh, J. & Rutter, E. H. 1983. The low temperature brittle–ductile transition in a quartzite and the occurrence of cataclastic flow in nature. *Geol. Rdsch.* **72**, 493–509.

Hadley, K. 1973. Laboratory investigation of dilatancy and motion on fault surfaces at low confining pressures. In: *Proc. Conf. Tectonic Problems of the San Andreas Fault System* (edited by Kovach, R. L. and Nur, A.), 427–435.

Hallbauer, D., Wagner, K. H. & Cook, N. G. W. 1973. Some observations concerning the microscopic and mechanical behavior of quartzite specimens in stiff, triaxial compression tests. *Int. J. Rock Mech. Min. Sci.* **10**, 713–726.

Handin, J. 1969. On the Coulomb–Mohr failure criterion. *J. geophys. Res.* **74**, 5343–5348.

Hanmer, S. K. 1982. Microstructure and geochemistry of plagioclase and microcline in naturally deformed granite. *J. Struct. Geol.* **4**, 197–213.

Hugman, R. H. H. & Friedman, M. 1979. Effects of texture and composition on mechanical behavior of experimentally deformed carbonate rocks. *Bull. Am. Ass. Petrol. Geol.* **63**, 1478–1489.

Kachanov, M. L. 1982. A microcrack model of rock inelasticity. *Mech. Mat.* **1**, 19–41.

Kranz, R. L. 1979. Crack growth and development during creep in Westerly granite. *Int. J. Rock Mech. Min. Sci.* **16**, 23–36.

Kranz, R. L. 1980. The effects of confining pressure and stress difference on static fatigue of granite. *J. geophys. Res.* **85**, 1854–1866.

Kranz, R. L. 1983. Microcracks in rocks, a review. *Tectonophysics* **100**, 449–480.

Kronenberg, A. K. & Shelton, G. L. 1980. Deformation microstructures in experimentally deformed Maryland diabase. *J. Struct. Geol.* **2**, 341–353.

McClintock, F. & Walsh, J. B. 1962. Friction on Griffith cracks in rocks under pressure. In *Proc. 4th U.S. Nat. Congr. App. Mech. II*, New York, ASME, 1015–1021.

Miller, F. S. 1937. Petrology of the San Marcos gabbro, Southern California. *Bull. geol. Soc. Am.* **48**, 1397–1426.

Mitra, G. 1978. Ductile deformation zones and mylonites: the mechanical processes involved in the deformation of crystalline basement rocks. *Am. J. Sci.* **278**, 1057–1084.

Mitra, G. 1984. Brittle to ductile transition due to large strains along the White Rock thrust, Wind River mountains, Wyoming. *J. Struct. Geol.* **6**, 51–61.

Montgomery, C. W. & Brace, W. F. 1975. Micropores in plagioclase. *Contr. Miner. Petrol.* **52**, 17–28.

Moss, W. C. & Gupta, Y. M. 1982. A constitutive model describing dilatancy and failure in brittle rock. *J. geophys. Res.* **87**, 2985–2998.

Murrell, S. A. F. & Digby, P. J. 1970. The theory of brittle fracture initiation under triaxial stress conditions. I. *Geophys. J. R. astr. Soc.* **19**, 309–334.

Nemat-Nasser, S. & Horii, H. 1982. Compression-induced nonplanar crack extension with application to splitting, exfoliation, and rock burst. *J. geophys. Res.* **87**, 6805–6822.

Nur, A. & Simmons, G. 1970. The origin of small cracks in igneous rocks. *Int. J. Rock Mech. Min. Sci.* **7**, 307–314.

Padovani, E., Shirey, S. B. & Simmons, G. 1982. Characteristics of microcracks in amphibolite and granulite facies grade rocks from southeastern Pennsylvania. *J. geophys. Res.* **87**, 8605–8630.

Paterson, M. S. 1978. *Experimental Rock Deformation—The Brittle Field*. Springer, New York.

Philofsky, E. M. & Hilliard, J. E. 1969. On the measurement of the orientation distribution of lineal and areal arrays. *Q. appl. Math.* **27**, 79–86.

Ramsay, J. G. 1980. The crack-seal mechanism of rock deformation. *Nature, Lond.* **284**, 135–139.

Richter, D. & Simmons, G. 1977. Microcracks in crustal igneous rocks: microscopy. In *The Earth's Crust*. Am. Geophys. Un. monograph **20**, 149–180.

Schock, R. N. & Heard, H. C. 1974. Static mechanical properties and shock loading response of granite. *J. geophys. Res.* **79**, 1662–1666.

Segall, P. & Pollard, D. D. 1983. Nucleation and growth of strike-slip faults in granite. *J. geophys. Res.* **88**, 555–568.

Shimada, M., Cho, A. & Yukutake, H. 1983. Fracture strength of dry silicate rocks at high confining pressures and activity of acoustic emission. *Tectonophysics* **96**, 159–172.

Smith, D. L. & Evans, B. 1984. Diffusive crack healing in quartz. *J. geophys. Res.* **89**, 4125–4135.

Sprunt, E. S. & Brace, W. F. 1974. Direct observation of microcavities in crystalline rocks. *Int. J. Rock Mech. Min. Sci.* **11**, 139–150.

Sprunt, E. S. & Nur, A. 1979. Microcracking and healing in granites: new evidence from cathodoluminescence. *Science, Wash.* **205**, 495–497.

Steif, P. S. 1984. Crack extension under compressive loading. *Engng Fracture Mech.* **20**, 463–473.

Stesky, R. M., Brace, W. F., Riley, D. K. & Robin, P-Y. F. 1974. Friction in faulted rock at high temperature and pressure. *Tectonophysics* **23**, 177–203.

Tapponnier, P. & Brace, W. F. 1976. Development of stress-induced microcracks in Westerly granite. *Int. J. Rock Mech. Min. Sci.* **13**, 103–112.

Trimmer, D., Bonner, B., Heard, H. C. & Duba, A. 1980. Effect of pressure and stress in water transport in intact and fractured gabbro and granite. *J. geophys. Res.* **85**, 7059–7071.

Tullis, J. & Yund, R. A. 1977. Experimental deformation of dry Westerly granite. *J. geophys. Res.* **82**, 5705–5718.

Underwood, E. E. 1970. *Quantitative Stereology*. Addison Wesley, Reading.

Walsh, J. B. 1981. Effect of pore pressure and confining pressure on fracture permeability. *Int. J. Rock Mech. Min. Sci.* **18**, 429–435.

Walsh, J. B. & Brace, W. F. 1984. The effect of pressure on porosity and the transport properties of rock. *J. geophys. Res.* **89**, 9425–9432.

Walsh, J. B. & Grosenbaugh, M. A. 1979. A new mode of analyzing the effect of fractures on compressibility. *J. geophys. Res.* **84**, 3532–3536.

Wang, H. F. & Simmons, G. 1978. Microcracks in crystalline rock from 5.3 km depth in the Michigan Basin. *J. geophys. Res.* **83**, 5849–5856.

Wawersik, W. R. & Brace, W. F. 1971. Post failure behavior of a granite and a diabase. *Rock Mech.* **3**, 61–85.

Wong, T-f. 1982a. Micromechanics of faulting in Westerly granite. *Int. J. Rock Mech. Min. Sci.* **19**, 49–64.

Wong, T-f. 1982b. Effects of temperature and pressure on failure and post-failure behavior of Westerly granite. *Mech. Mat.* **1**, 3–17.

Wong, T-f. 1982c. Shear fracture energy of Westerly granite from post-failure behavior. *J. geophys. Res.* **87**, 990–1000.

Wong, T-f. in press. Geometric probability approach to the characterization and analysis of microcracking in rocks. *Mech. Mat.*